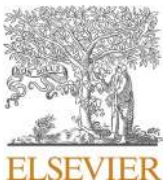
Ecological Indicators 186 (2026) 114888



Contents lists available at ScienceDirect

Ecological Indicators

journal homepage: www.elsevier.com/locate/ecolind



Cost-effective monitoring of a rare Pannonian steppe plant using drone imagery

László Bakacsy [a,*], Zalán Tobak [b], László Mucsi [b], Boudewijn van Leeuwen [c], Csaba Biró [d], József Szatmári [b]

[a] Department of Plant Biology, University of Szeged, Közép fasor 52, H-6726 Szeged, Hungary
[b] Department of Atmospheric and Geospatial Data Sciences, University of Szeged, Egyetem utca 2-6, H-6722 Szeged, Hungary
[c] Bay Zoltán Nonprofit Ltd. for Applied Research, Division of Biotechnology, H-6726 Szeged, Derkovits fasor 2, Hungary
[d] Kiskunsag National Park Directorate, Liszt Ferenc utca 19, H-6000 Kecskemét, Hungary

ARTICLE INFO

Keywords:
Drone (UAV)
Image processing
Protected species
QGIS
Sedum urvillei subsp. *hillebrandtii*
Spectral discrimination
Vegetation indices

ABSTRACT

Efficient monitoring of rare and protected plant species is essential for biodiversity conservation. This study evaluates a cost-effective and non-invasive UAV-based method using RGB vegetation indices derived from the red, green and blue image channels to enhance vegetation colour contrast to detect *Sedum urvillei* subsp. *hillebrandtii*, a protected Pannonian subendemic species. A fixed-wing drone equipped with an RGB camera surveyed an 8.5-ha open sandy grassland within the Kiskunság National Park, Hungary, during the species' peak flowering period. Three RGB-based vegetation indices – Triangular Greenness Index (TGI), Colour Index of Vegetation Extraction (CIVE), and Red-Green Ratio (RGR) – were applied to an orthophoto mosaic to classify flowering individuals. Negative masking using RGR significantly improved the classification accuracy of both TGI and CIVE. Statistical analysis revealed high overall accuracy (up to 99.3%) and specificity (>99%) for the CIVE–RGR and TGI–RGR combinations, while sensitivity increased from 79.1% to 89.0% after applying RGR-based masking. Automated thresholding using the Otsu method increased sensitivity but resulted in reduced specificity and overall classification stability due to increased false positive detections. These results demonstrate that spectral differentiation based on floral coloration can enable reliable species-level detection using low-cost RGB imagery under favorable flowering and illumination. Compared to complex multispectral and hyperspectral approaches, this method offers a reproducible, rapid, and scalable solution for conservation monitoring. However, its applicability remains restricted to the flowering period. The methodology may be transferable to other visually distinctive flowering species, provided that species-specific threshold validation is performed, and may support habitat monitoring and pollinator-related ecological studies in Pannonian steppe habitats.

1. Introduction

Recent advances in drone or UAV (Unmanned Aerial Vehicle) technology and remote sensing have led to a revolution in the field of ecological monitoring, providing new tools for accurate and efficient data collection (Nowak et al., 2018; Bakó, 2013). The use of drones equipped with high-resolution cameras enables the conducting of large-scale vegetation surveys with minimal habitat disturbance. Furthermore, this method provides a cost-effective and rapid assessment approach for a comprehensive survey of a given area. The ability to capture detailed images and apply vegetation indices enables researchers to identify and monitor plant species with high precision (Cruzan et al., 2016; Nowak et al., 2018).

It is imperative to recognize the significance of species that are indicative of grassland degradation in facilitating our comprehension of ecological succession and the provision of early warnings concerning ecosystem decline. These species are highly valuable for examining how grasslands react to pressures such as grazing, anthropogenic impacts, and other degradation-inducing factors (Liu et al., 2011; Wang et al., 2024). The tracking of variations in key attributes of these species, including their relative importance and dominance, has become a critical method for evaluating the extent of grassland degradation (Zhang

* Corresponding author.
E-mail addresses: bakacsy.laszlo@szte.hu (L. Bakacsy), tobak.zalan@szte.hu (Z. Tobak), mucsi.laszlo@szte.hu (L. Mucsi), leeuwen@bayzoltan.hu (B. van Leeuwen), birocs@knp.hu (C. Biró), szatmari.jozsef@szte.hu (J. Szatmári).

https://doi.org/10.1016/j.ecolind.2026.114888
Received 8 January 2026; Received in revised form 23 March 2026; Accepted 15 April 2026
1470-160X/© 2026 The Author(s). Published by Elsevier Ltd. This is an open access article under the CC BY license (http://creativecommons.org/licenses/by/4.0/).

et al., 2020). The monitoring and conservation of rare and endemic plant species is essential for maintaining the biodiversity and ecological balance of grassland environments (Wang et al., 2022; Bakó et al., 2024). Accurate and timely data on the distribution and health of rare or endemic plant populations can inform conservation actions such as habitat protection, restoration efforts, and climate adaptation strategies (Rominger and Meyer, 2019; Reckling et al., 2021; Bates et al., 2022). By utilizing drone technology and advanced analytical methods, these studies contribute to the broader goal of conserving several threatened ecosystems and their unique biodiversity (Jiménez López and Mulero-Pázmány, 2019).

RGB indices derived from the red, green, and blue spectral bands are commonly used in agriculture and forestry to assess plant health, density, and distribution (Arok et al., 2025; Bakó, 2013; Sun et al., 2025). By combining the RGB colour channels, a variety of vegetation indices can be calculated that are sensitive to the spectral characteristics and condition of plants. This spectral discrimination is beneficial for identifying and mapping individual species, especially in heterogeneous habitats where multiple plant species coexist (Chaity et al., 2024). Using drones equipped with high-resolution RGB cameras; researchers can conduct large-scale surveys quickly and efficiently; producing detailed images that enable the application of various RGB-based vegetation indices; such as the Excess Green Index (ExG); the Simple Blue-Green Ratio (BGR); and the Visible Atmospherically Resistant Index (VARI). These indices can help to isolate the spectral signatures of target species; facilitating accurate detection and population estimation (Borah et al., 2025). In the present study; three RGB-based vegetation indices widely used in vegetation analysis – the Triangular Greenness Index (TGI); the Colour Index of Vegetation Extraction (CIVE); and the Red-Green Ratio (RGR) – were selected to detect flowering individuals of the target species. This method is not only non-invasive but also cost-effective (no need for expensive camera-equipped drones); reducing the need for labour-intensive ground surveys; while providing high spatial resolution data essential for monitoring biodiversity and guiding conservation efforts; although its effectiveness may depend on species visibility; phenological stage; and environmental conditions (Arok et al., 2025; Sun et al., 2025).

The flowers of plant species during their flowering season present a distinctive opportunity for the use of RGB indices for species detection by drones (Cruzan et al., 2016; Nowak et al., 2018; Bakacsy et al., 2023). The bright colors of flowers, particularly during the flowering season, provide excellent contrast against the background vegetation, enabling accurate and effective species detection. RGB indices, derived from the specific wavelengths of light captured by the drone's cameras, can be fine-tuned, and good results can be achieved even by using simple indices or methods (Bakacsy et al., 2023). Machine learning algorithms have shown potential in flower classification tasks in other studies; however; this study focuses exclusively on RGB index-based approaches (Gröschler and Oppelt, 2022). The flower-based monitoring not only provides insight into the population size and health of the species but also helps to evaluate the effectiveness of conservation efforts. Consequently; species identification based on flowers or inflorescences has already been successfully applied to numerous invasive plant species (Bakacsy et al., 2023). Furthermore; the data obtained can be utilized to ascertain the sufficiency of both the quality and quantity of available food for pollinators; including bees and butterflies (Tabor, 2022). It is notable that; except for a few studies; there is a paucity of information on the monitoring of rare; protected plant species based on flowers using drones (Gröschler and Oppelt, 2022). Additionally; there is a lack of research on the use of RGB-based monitoring. Such an approach would contribute significantly to our understanding and conservation of rare species and flowers. These approaches facilitate the identification of the most reliable and efficient method for monitoring populations of rare or endemic plant species; thereby providing valuable insights for future ecological research. *Sedum urvillei* subsp. *hillebrandtii* (Fenzl) D.A. Webb (Crassulaceae) is a Pannonian subendemic perennial species characteristic of open sandy grasslands in the Danube Basin and adjacent regions (Simon, 2000; Király, 2009; ICN, 2025). The species forms compact; low-growing clumps composed of short shoots that produce dense cymose inflorescences with bright yellow flowers (Fig. 1) during early to mid-summer (June–July). During this flowering period the clustered inflorescences create visually distinct patches that contrast strongly with the surrounding gray-green grassland matrix; making the species particularly suitable for detection using high-resolution RGB imagery. Such strong chromatic contrast between flowers and background vegetation has been shown to facilitate UAV-based identification of plant species using simple colour-derived indices (Cruzan et al., 2016; Bakacsy et al., 2023; Gröschler and Oppelt, 2022; Tabor, 2022). Ecologically, *S. urvillei* subsp. *hillebrandtii* is typically associated with well-preserved open sand grasslands of the Pannonian steppe (Natura 2000 habitat type 6260), where it occurs in sparsely vegetated microsites with high light availability and limited competition. Because its populations are primarily restricted to structurally intact sandy grassland patches, the species is considered a useful indicator of high-quality habitat conditions in these ecosystems (Simon, 2000; Király, 2009; Biró, 2023). Monitoring the spatial distribution and abundance of this species can therefore provide indirect information about habitat status and vegetation dynamics in conservation areas. UAV-based mapping of flowering plants has also been used to quantify floral resources and to relate floral availability to pollinator community structure, highlighting the broader ecological relevance of flower-based remote sensing approaches (Tabor, 2022). Although the method presented here focuses on a single target species, the underlying approach is not restricted to *Sedum*. UAV-based detection using RGB indices can be transferable to other plant species that exhibit similarly distinctive flowering phenology, compact patch structure, and strong colour contrast against surrounding vegetation. Consequently, the species serves as a suitable model organism for testing cost-effective RGB-based workflows for species-level monitoring in heterogeneous grassland communities.

For this study, a fixed-wing drone was used, equipped with RGB cameras to survey populations of *Sedum urvillei* subsp. *hillebrandtii*, which can provide critical information for nature conservation. The bright yellow flowers of the species make it easier to identify during blooming periods. Therefore, we aimed to determine which RGB indices can identify the species with high efficiency during flowering, in order to develop a cost-effective population estimation workflow for conservation monitoring. Although the present analysis focuses on a single target species, the methodological framework may also be applicable to other flowering plant species with similarly distinctive spectral characteristics.

2. Materials and methods

2.1. Study site

A survey of the protected species was conducted on 27th July 2023 using a drone in the open sandy grasslands situated in the vicinity of Lake Kolon, which forms part of the Kiskunsági National Park. Lake Kolon represents a significant feature within the Kiskunság National Park in Hungary, forming part of the Pannonian biogeographical region, and includes extensive wetland habitats. The area is characterized by a mosaic of diverse habitats, each supporting a unique assemblage of plant species. Lake Kolon is in a late successional phase, with artificial open water surfaces. Consequently, although the lake is frequently described as a marsh due to its shallow waters and extensive reed beds, it serves as a vital hydrological entity in the region. The mean depth is 1 m, although former peat mining pits have created areas with depths of 2–3 m. The dominant vegetation type comprises extensive areas of common reed (*Phragmites australis* (Cav.) Trin. ex Steud.) and sedge (*Carex* spp.) beds, which play a pivotal role in water purification and provide habitat for a multitude of bird species, particularly during migration periods. While *Nymphaea alba* L. (white water lily), *Stratiotes aloides* L. (water

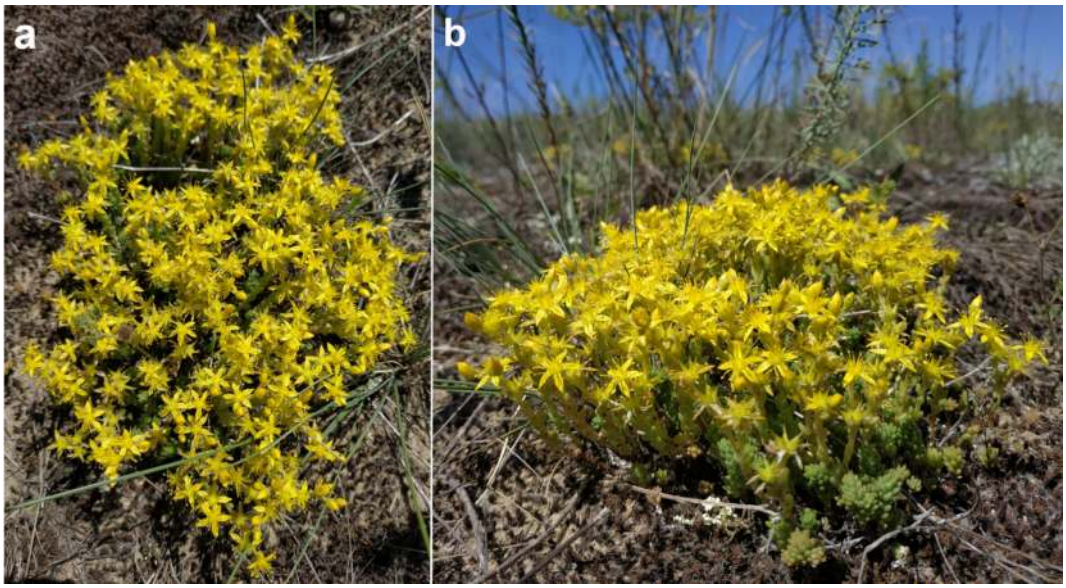


Fig. 1. A blooming *Sedum urvillei* subsp. *hillebrandtii* patch, approximately the size of a palm, viewed from (a) above and (b) side.

soldier), and *Utricularia vulgaris* L. (common bladderwort) are found in the open water (Tóth, 1996; Sipos et al., 2014).

The transition zones adjacent to the reed beds host a variety of wet meadow communities. Lake Kolon's diverse habitats render it a valuable ecosystem within the Kiskunság National Park. These meadows are interspersed with patches of alkaline fens and tussock sedges, which contribute to the high biodiversity of the area. In the surrounding terrestrial zones, one can find remnants of steppe grasslands, characterized by various drought-resistant endemic species (Tóth, 1996; Bölöni et al., 2011). The surveyed area's habitat is part of the endemic open sand grasslands, also known as Pannonian steppes, which hold significant importance under the European Union Habitat Directive (Natura 2000 code: 6260) (Bölöni et al., 2011). The surveyed stand covered an area of 8.5 ha (Fig. 2). In addition to the target species, the stand exhibited a notable prevalence of other native plant species that are characteristic of open sandy grasslands, including *Euphorbia seguieriana* Neck. (Seguier's spurge), *Festuca vaginata* Waldst. et Kit. (Hungarian fescue), *Fumana procumbens* (Dun.) Gren et Godr. (trailing fumana), *Stipa borysthenica* Klokov (Pontic feather grass), *Koeleria glauca* (Sperg.) DC. (blue hair grass) and *Alkanna tinctoria* (L.) Tausch (dyer's alkanet). Furthermore, the lichen community of the habitat is of considerable significance. The location of this stand is illustrated in Fig. 2.

2.2. Drone survey

A larger population of *Sedum urvillei* subsp. *hillebrandtii* was surveyed in the vicinity of Lake Kolon using a senseFly eBee X fixed-wing drone. This drone has a wingspan of 116 cm, a weight range of 1.1–1.4 kg depending on the payload, and a maximum flight duration of 45 min. The drone is capable of maintaining a radio connection at a distance of up to 3 km. The RGB camera employed during the flights was a senseFly S.O.D.A., which supports RTK/PPK, has a resolution of 5472 × 3648 pixels, a global shutter speed ranging from 1/30 to 1/2000 s, and captures images in JPEG or DNG format. The central wavelengths of the RGB bands were 660 nm (red), 520 nm (green), and 450 nm (blue).

A single flight was conducted over the vegetation stand using the drone-mounted senseFly S.O.D.A. camera, following predefined flight paths. The average speed during the flights was 13 m/s. In order to maximize image overlap and thus enhance data accuracy for the sample area, the length of the flight paths was extended, thereby increasing the photographed area. The flight parameters for the vegetation stand were as follows: the flight altitude was 53 m AGL (above ground level), the flight duration was 15 min, and a total of 476 images were captured. These images had a resolution of 5 cm/pixel and featured 60% longitudinal and 80% transverse overlap. The weather during the flights and the preceding week was sunny and dry.

2.3. Data processing methods

An orthophoto mosaic of the stand was created from the aerial photographs using Agisoft Metashape Professional 1.5.4 (Agisoft, 2020). In the Agisoft programme, no ground reference points were used during the working process, but the so-called onboard references (OtF stands for on-the-fly reference method) were used. The X, Y, and Z coordinates of the image centres were measured with geodetic accuracy using onboard GNSS, with correction signals applied via post-processing steps.

We selected 10 sample areas of 10 m × 10 m on the orthophotos of the stand. The main consideration for selecting the sample areas was that they should be randomly and spatially distributed (Fig. 2). In these sample areas, the representation of *Sedum* patches was variable. The workflow was carried out in the QGIS environment (QGIS Development Team, 2021).

2.4. Application of RGB indices and validation of classification

Vegetation indices commonly used in agriculture and forestry, calculated from the RGB image bands, were used to identify patches of the protected species. To detect vegetation patches and to identify *S. urvillei* subsp. *hillebrandtii* with maximum efficacy, three RGB-based vegetation indices known from the literature were selected and calculated: the Triangular Greenness Index (TGI), the Colour Index of Vegetation Extraction (CIVE), and the Red-Green Ratio (RGR). The indices were computed separately for each sample area using the Raster Calculator tool of QGIS 3.40.7.

The CIVE index, which is primarily employed to enhance the colour intensity of vegetation (Kawashima and Nakatani, 1998), was calculated using the following formula (Eq. 1):

$$CIVE = 0.441R - 0.811G + 0.385B + 18.787 \quad (1)$$

The TGI index, which relies on a triangulation-based approach to capture the greenness of vegetation (Hunt et al., 2011), was computed as follows (Eq. 2):

$$TGI = -0.5\left[(\lambda_r - \lambda_r)(R_r - R_g) - (\lambda_r - \lambda_g)(R_r - R_b)\right] \quad (2)$$

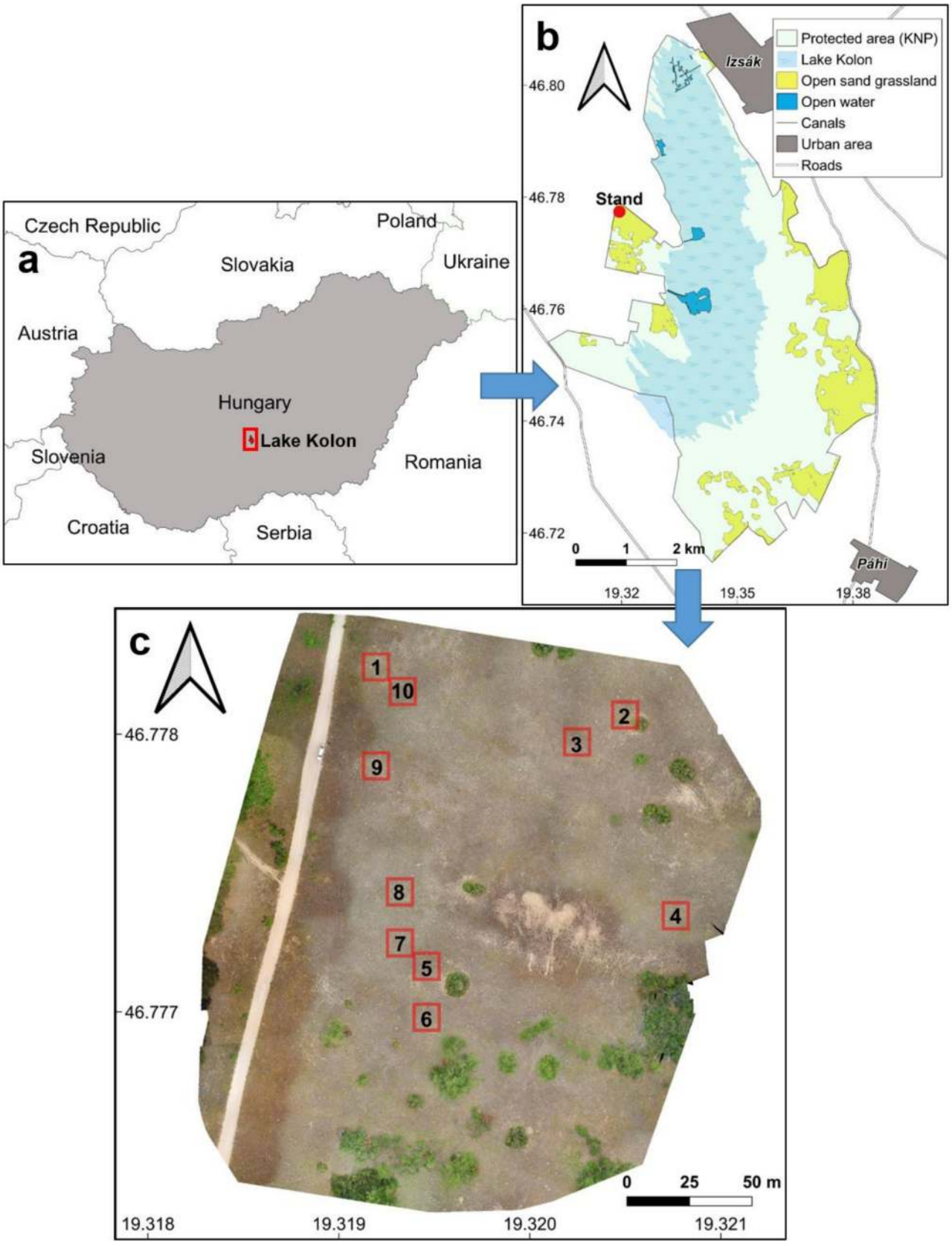


Fig. 2. The study site is located (a) in Hungary, and (b) the chosen stand is connected to open sand grasslands. The orthomosaics of the stand (c) illustrate the locations of the randomly selected 10 m × 10 m sample areas (1−10).

where λ_r, λ_g, λ_b are central wavelength of red, green, and blue bands, respectively, R_r, R_g, and R_b are the reflectances for red, green, and blue bands, respectively.

The third index applied was the Red-Green Ratio (RGR), a metric frequently employed for the assessment of plant stress and physiological status (Gamon and Surfus, 1999). The formula for the RGR is as follows (Eq. 3):

$$RGR = \frac{R}{G} \tag{3}$$

Based on the index values, the generation of grayscale raster maps was undertaken for each sample area. Subsequently, an optimal threshold range was defined for each index through visual assessment. This range was determined to optimise the distinction between flowering individuals of the target species and the background. These thresholds were then applied to reclassify the raster layers into binary format, where the patches of the target species were consistently represented as 1 (and the background as 0 or NoData). In cases where the thresholding of a given index resulted in an inverse classification (i.e. lower values indicating the presence of the species), the binary map was inverted to ensure consistency. The resulting binary rasters were then vectorised using the GDAL Polygonize tool in QGIS.

The threshold values were initially determined by visual inspection of the vegetation index rasters within the sample areas. To support the objectivity of the threshold selection, histogram distributions of vegetation index values were analyzed for each sample area. In both indices, vegetation pixels formed a dominant peak in the histogram distributions, while background pixels occurred mainly in the lower (CIVE) or higher (TGI) value ranges. The selected thresholds correspond to the transition zone between these distributions, where the frequency of background pixels rapidly declines and vegetation pixels begin to dominate. To further evaluate the robustness of threshold selection, automated threshold estimation was performed using the Otsu algorithm (Otsu, 1979) for all sample areas. The Otsu-derived thresholds were used for comparison with the visually determined threshold values and to assess the consistency between manual and automated threshold selection approaches. The RGR index was used as a negative mask variable to remove potential false positive pixels from the CIVE – TGI based classification. Therefore, its threshold was applied as a conservative filtering criterion rather than being derived from vegetation-background separation.

The polygons generated by RGR index were used to exclude non-target vegetation features. However, these features were sometimes falsely identified by other indices (CIVE, TGI) as positives. Consequently, the final prediction layers were created by subtracting the RGR-based polygons from the CIVE and TGI-derived polygon layers (QGIS "Geoprocessing Tools→Difference"), thereby enhancing classification specificity or accuracy. For the purpose of validation, all flowering patches of the target species were manually delineated at each sample area and used as independent reference layers for calculating the confusion matrix elements. The validation was carried out on samples that were not used to determine the threshold values for slicing the different indices, ensuring that accuracy metrics were derived from independent data. The following logical operations were applied using QGIS "Geoprocessing Tools": True Positive (TP): The intersection between the predicted (index-based) and actual (manual) polygon layers. A 'false positive' (FP) is characterized by a discrepancy between the predicted layer and the overlay, with the overlay being the actual (manual) layer. False Negative (FN): The reverse difference method involves the use of the actual layer as the input, with the predicted layer (overlay) serving as the reference. True Negative (TN): Initially, a symmetrical difference was created between the total sample area polygon and the manual delineation to define the real background patches. These patches were then intersected with the index-based layer. Subsequently, the resulting values were utilized to calculate accuracy, sensitivity (recall), and specificity for each sample area. The complete workflow of index calculation, thresholding, and post-processing is illustrated in Fig. 3.

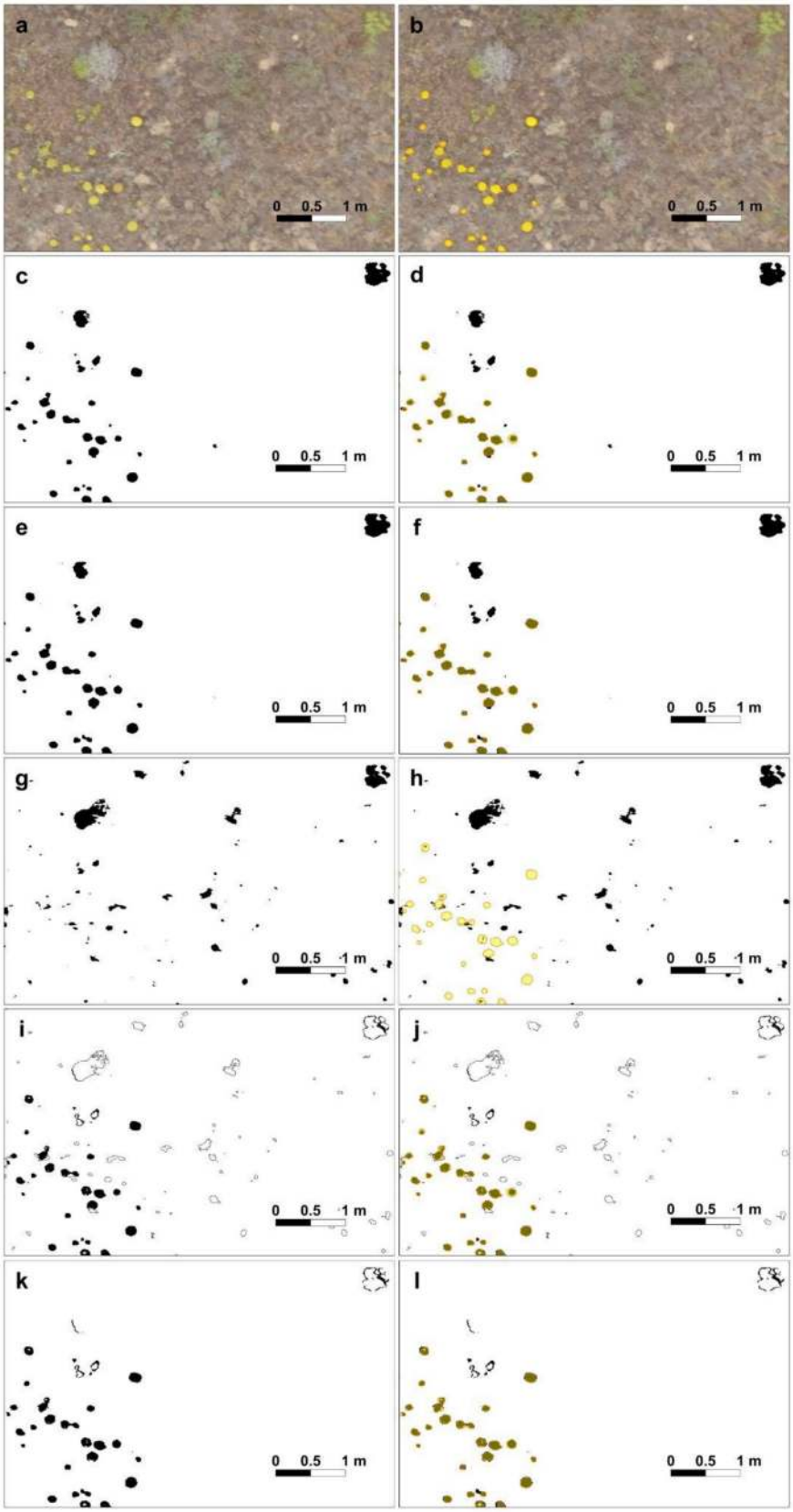
2.5. Statistical analysis

To compare the classification performance of the RGB-based vegetation indices (CIVE, TGI, CIVE–RGR, and TGI–RGR) under different thresholding approaches (visual and Otsu-based), statistical analyses were conducted using accuracy, sensitivity, specificity, and Intersection over Union (IoU) metrics calculated for each of the ten sample areas. As all index–threshold combinations were evaluated across the same sample areas, the data represented repeated measurements. Given the relatively small sample size and to avoid assumptions of normality, differences among methods were assessed using the non-parametric Friedman test, followed by Dunn's multiple comparisons post hoc test to identify pairwise differences between index–threshold combinations. Statistical evaluation was conducted using GraphPad Prism version 8.0.1.244 for Windows (GraphPad Software, La Jolla, CA, USA). The level of significance was set to 0.05, and *p*-values above this threshold were considered non-significant.

3. Results

The value ranges of the index maps generated from the orthophoto mosaic showed significant differences among the applied RGB-based vegetation indices. The CIVE values ranged between -28.92 ± 4.473 and 32.32 ± 16.289 across the examined sample areas, while the TGI varied between -764 ± 1347.4 and 8211.5 ± 707.216. In contrast, the Red-Green Ratio (RGR) covered a narrower interval, ranging between 0.887 ± 0.03 and 1.473 ± 0.635 (Table 1). The distribution of values for each index is indicative of their differing spectral sensitivities, which facilitates the effective distinction of the flowering patches of the target species from the background vegetation. Representative classification outputs are shown in Fig. 3.

Threshold values were determined for each sample area using both visual interpretation and an automated Otsu-based approach (Table 2). For the visually defined thresholds, relatively consistent values were obtained across sample areas, with mean thresholds of 6.5 ± 1.27 for CIVE and 2450 ± 250.55 for TGI (Table 2). The RGR index was applied as a fixed upper threshold (1.207 ± 0.016) and used exclusively as a negative mask to exclude non-target vegetation. In contrast, Otsu-derived thresholds showed greater variability among sample areas, particularly for the TGI index (1500 ± 579.2), while CIVE thresholds were moderately variable (14.36 ± 3.54; Table 2). The Otsu thresholds generally differed from the visually selected values, reflecting the data-driven and distribution-dependent nature of the automated method. Importantly, both visual and Otsu-derived thresholds were located within the transition zone of the histogram distributions separating vegetation and background pixels (Fig. 4), indicating that the visual threshold selection was consistent with objective, histogram-based criteria. While the Otsu method provided an objective and reproducible thresholding approach, the visually defined thresholds were intentionally more conservative, retaining only pixels with strong vegetation signals. Otsu-based thresholding consistently increased sensitivity, but this improvement was accompanied by reduced specificity, indicating a trade-off between detection rate and false positive errors. The quantitative performance evaluation of the four RGB-based index combinations (CIVE, TGI, CIVE–RGR, TGI–RGR) and thresholds (visual and Otsu) were based on three key metrics – accuracy, sensitivity, and specificity – calculated from confusion matrices for each of the ten sample areas. The findings demonstrated that the subtraction of the RGR index enhanced the accuracy and reliability of classification in both CIVE and TGI scenarios. The spatial patterns of classification outputs derived from the different index–threshold combinations are illustrated in Fig. 5. Visual inspection confirms that RGR-based masking reduces false positive



(caption on next page)

Fig. 3. A section of the third sample area shown on the orthophoto (a), and complemented with manually digitized polygons (b). Binary maps generated by thresholding the applied RGB-based vegetation indices (c, e, g), and the same areas with the contours of the manual polygons overlaid (d, f, h). The examples present the results of the CIVE (c–d), TGI (e–f), and RGR (g–h) indices, respectively. In the CIVE and TGI binary maps, black indicates patches of the target species (*Sedum urvillei* subsp. *hillebrandtii*), while white represents background vegetation. The RGR index is not directly sensitive to the target species but was used to filter out patches incorrectly classified as target species by CIVE or TGI. Panels (i–j and k–l) show the final classification outputs obtained after applying RGR-based negative masking to the CIVE (i–j) and TGI (k–l) maps, respectively. Yellow contours represent the manually digitized polygons in all cases. The presented classification results are based on visually defined thresholds; Otsu-based thresholding results are not shown here for clarity but are quantitatively evaluated in Figs. 4–8. (For interpretation of the references to colour in this figure legend, the reader is referred to the web version of this article.)

Table 1
Basic statistics (min, max, mean ± SD) of the three RGB-based vegetation indices.

Sample area	CIVE		TGI		RGR	
	min	max	min	max	min	max
S1	−25.848	24.908	−140	7650	0.923	1.224
S2	−26.906	28.671	−510	7880	0.859	1.46
S3	−33.808	28.289	−365	9045	0.911	1.317
S4	−32.837	78.508	−4580	8930	0.844	3.266
S5	−30.266	28.902	−545	7670	0.87	1.285
S6	−24.57	27.858	−450	8075	0.885	1.226
S7	−26.542	26.495	−215	7645	0.895	1.201
S8	−37.636	25.427	−205	9595	0.893	1.173
S9	−25.743	27.007	−295	7810	0.934	1.313
S10	−25.063	26.931	−335	7815	0.856	1.26
Mean	−28.92 ± 4.473	32.3 ± 16.289	−764 ± 1347.4	8211.5 ± 707.216	0.887 ± 0.03	1.473 ± 0.635
Total index range		61.22		8975.5		0.585

Table 2
Threshold values applied for RGB-based vegetation indices across the ten sample areas using visual and Otsu-based thresholding approaches.

Study area	Visual threshold			Otsu threshold	
	CIVE ≥	TGI ≤	RGR ≤	CIVE ≥	TGI ≤
S1	6	2200	1.02	13.08	1805
S2	7	2700	1.02	9.362	2250
S3	5	2600	1.03	20.247	650
S4	6	2700	1.02	9.247	2195
S5	7	2500	1.04	14.654	1835
S6	8	1900	1.05	13.055	1835
S7	5	2500	1	16.794	950
S8	6	2600	1.01	17.82	780
S9	9	2300	1.05	16.294	1165
S10	6	2500	1.03	13.049	1530
Mean ± SD	6.5 ± 1.269	2450 ± 250.554	1.207 ± 0.016	14.36 ± 3.537	1500 ± 579.2

For each method, threshold values are reported for the CIVE and TGI indices, while the RGR index was used exclusively as a negative masking variable. Mean values are presented with ± standard deviations (SD).

detections, while Otsu-based thresholding results in a higher number of detected patches, including non-target areas.

Accuracy values were consistently high for all index combinations when visually defined thresholds were applied, with median values exceeding 97% across all sample areas (Fig. 6, Supplementary Table S1). No statistically significant differences were detected among the visual threshold-based methods (CIVE, TGI, CIVE–RGR, and TGI–RGR; Friedman test with Dunn's post hoc comparisons). In contrast, the use of Otsu-based thresholds resulted in lower and more variable accuracy values. Statistical comparisons revealed that several visual threshold-based approaches significantly outperformed their Otsu-based counterparts. In particular, TGI-based classification using visual thresholds showed significantly higher accuracy than TGI with Otsu thresholding (97.51% ±1.00%, 89.69% ±8.09%, $p = 0.0284$). Similarly, both CIVE–RGR and TGI–RGR approaches with visual thresholds (99.29% ±0.31% and 98.98% ±0.487%) achieved significantly higher accuracy compared to their Otsu-based equivalents (92.78% ±6.36% and 92% ±7.64%) ($p < 0.0001$ in both cases; Fig. 6, Supplementary Table S1). No significant differences were observed between CIVE–RGR and TGI–RGR within either thresholding approach, indicating comparable performance between the two index combinations.

Sensitivity values varied more substantially among methods compared to accuracy (Fig. 7, Supplementary Table S2). Under visually defined thresholds, TGI-based approaches generally achieved higher sensitivity values than CIVE-based methods. In particular, visual TGI–RGR showed the highest sensitivity (90.23% ±5.41%), and a statistically significant difference was observed between visual CIVE and visual TGI–RGR (79.1% ±5.71% and 90.23% ±5.41%; $p = 0.0391$). Additionally, visual CIVE–RGR exhibited significantly lower sensitivity compared to Otsu based TGI (88.99% ±5.75%, 97.53% ±2.52%; $p = 0.0146$), indicating a consistent advantage of TGI-based indices under visual thresholding. In contrast, Otsu-based thresholding resulted in generally high sensitivity values across all index combinations, with reduced variability among methods. A significant difference was detected between TGI and CIVE–RGR (97.53% ±2.52%, 87.87% ± 5.81%; $p = 0.0017$), while other pairwise comparisons were not statistically significant (Fig. 7, Supplementary Table S2).

Specificity values were consistently high under visually defined thresholds, with all index combinations exceeding 97% and showing low variability among sample areas (Fig. 8, Supplementary Table S3). The application of the RGR-based masking significantly improved specificity for both indices with visual thresholding, as CIVE–RGR (99.39% ±0.29%) and TGI–RGR (99.08% ±0.5%) achieved significantly higher values compared to their respective base indices (both $p < 0.0001$;

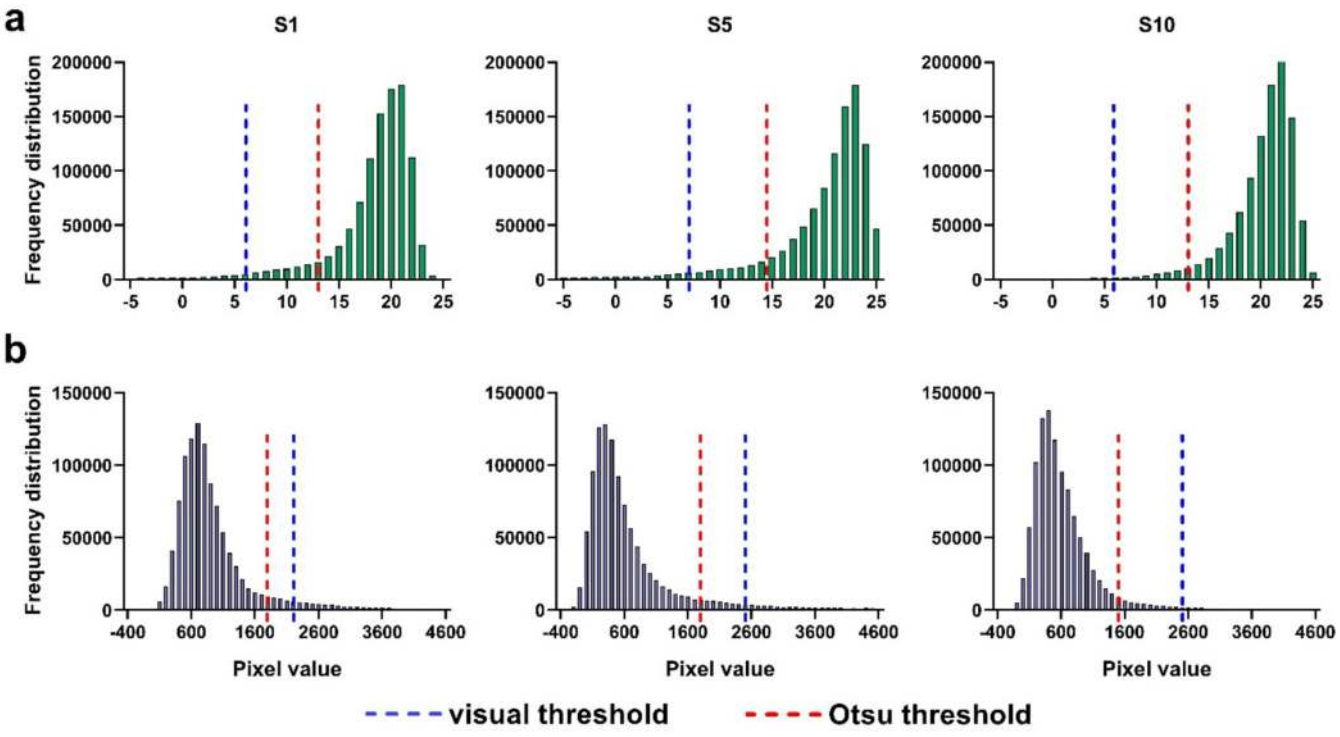


Fig. 4. Histogram-based threshold determination for vegetation indices. Histogram distributions of (a) CIVE and (b) TGI values derived from RGB imagery for three representative sample areas (S1, S5, S10). The dashed red lines indicate the automatically determined thresholds calculated using the Otsu algorithm. The dashed blue lines indicate the visually selected thresholds, used in the classification correspond to the same transition zone of the histogram distributions separating vegetation and background pixels. (For interpretation of the references to colour in this figure legend, the reader is referred to the web version of this article.)

Fig. 8, Supplementary Table S3). While, Otsu-based thresholding resulted in a noticeable decrease in specificity, accompanied by increased variability across sample areas. Significant differences were observed between visual and Otsu-based thresholding for both CIVE and TGI ($p = 0.0284$ and $p = 0.0391$; Fig. 8, Supplementary Table S3), indicating that the automatic thresholding approach led to a less reliable exclusion of non-target areas. For visual thresholding CIVE, this proportion increased from 97.91% ± 0.95%, for visual TGI, it improved from 97.65% ± 1.01%. While for Otsu based CIVE and TGI specificity were 89.43% ±6.95% and 89.57% ±8.24% (Fig. 8, Supplementary Table S3). No statistically significant differences were detected among the index combinations under Otsu thresholding (Fig. 8, Supplementary Table S3), suggesting that the choice of index had a reduced influence on specificity when automatic thresholding was applied.

The comparison of classification performance based on Intersection over Union (IoU) revealed substantial differences among thresholding approaches. Visual thresholding combined with RGR masking resulted in the highest IoU values across all sample areas. In contrast, Otsu-based thresholding produced significantly lower IoU values. Statistical analysis using the Friedman test with Dunn's post hoc comparisons confirmed that both CIVE-RGR and TGI-RGR visual thresholds (0.729 ± 0.197 and 0.687 ± 0.214) significantly outperformed Otsu-based thresholds (0.201 ± 0.122 and 0.215 ± 0.154) ($p < 0.0001$–0.0024; Fig. 9, Supplementary Table S4). No significant differences were observed between certain method pairs, indicating that the application of RGR masking alone did not consistently improve classification performance when combined with Otsu thresholding (Fig. 9 and Supplementary Table S4).

The negative masking approach, utilizing the RGR index to filter out non-target vegetation patches, improved classification performance, particularly in terms of sensitivity and specificity. When combined with visually defined thresholds, this approach yielded the highest accuracy and IoU values across all sample areas. These results indicate that RGR-based masking is an effective post-classification refinement step for improving the performance of RGB-based vegetation indices in UAV-assisted monitoring of protected plant species, such as *Sedum urvillei* subsp. *hillebrandtii*.

4. Discussion

This study demonstrates that RGB-based UAV imagery combined with vegetation indices can effectively detect populations of Sedum urvillei subsp. hillebrandtii during peak flowering. The combination of CIVE, TGI, and RGR masking achieved high classification performance (accuracy >99%), indicating that floral spectral contrast enables reliable species-level detection using RGB data.

To facilitate a direct comparison with previously published UAV-based plant monitoring studies cited in this manuscript, the main methodological characteristics and reported performance metrics of these approaches are summarized in Table 3. The comparison shows that UAV-based plant monitoring ranges from simple RGB index workflows to more complex multispectral or machine-learning approaches. The method presented in this study is positioned at the low-cost, low-complexity end of this spectrum, relying on a standard RGB sensor and a limited set of visible-band vegetation indices (CIVE and TGI) combined with an RGR-based negative mask and straightforward GIS operations. Under the tested conditions, this approach achieved very high classification performance, with overall accuracy exceeding 99% and high spatial agreement with manually delineated patches. At the same time, Table 3 also illustrates that methodological complexity and sensor sophistication are often determined by ecological context. For example, Gröschler and Oppelt (2022) achieved an F1-score of 0.99 using multispectral imagery and random forest classification; while Tabor (2022) employed multiple spectral indices and texture features to map floral resources. In contrast; manual approaches such as that used by Bakó et al. (2024) can achieve good detection accuracy but require considerable human effort. These comparisons indicate that RGB-based approaches can provide reliable and scalable solutions when target species

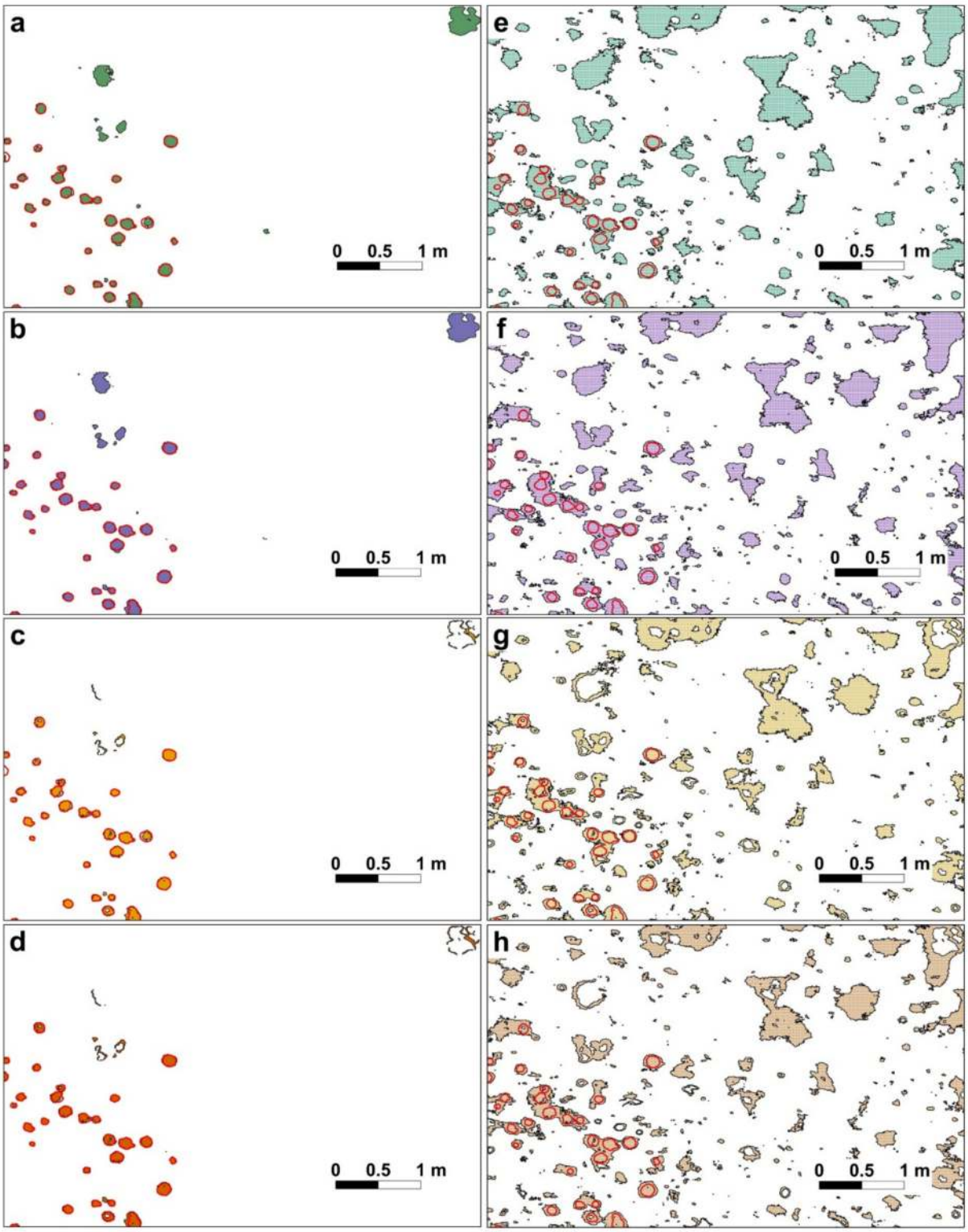


Fig. 5. Spatial comparison of classification outputs obtained using different vegetation index–threshold combinations for a representative sample area (S3). Red outlines indicate manually delineated *Sedum* patches (reference data). Panels (a–d) show results based on visually defined thresholds: (a) CIVE, (b) TGI, (c) CIVE–RGR, and (d) TGI–RGR. Panels (e–h) present results derived from Otsu-based thresholding: (e) CIVE, (f) TGI, (g) CIVE–RGR, and (h) TGI–RGR. The comparison illustrates the effect of thresholding strategy and RGR-based masking on classification performance. (For interpretation of the references to colour in this figure legend, the reader is referred to the web version of this article.)

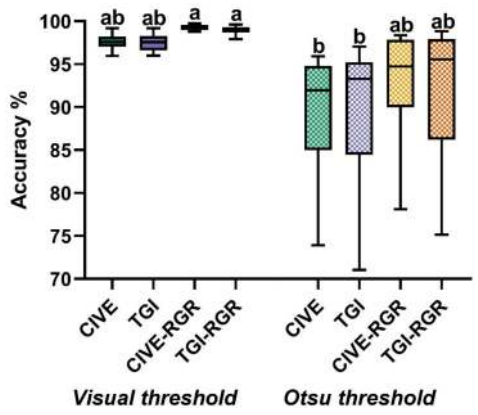


Fig. 6. Overall classification accuracy (%) of the four RGB index combinations (CIVE, TGI, CIVE–RGR, and TGI–RGR) under visual and Otsu-based thresholding across the ten sample areas. Different letters above the boxes indicate statistically significant differences among groups (Dunn's test, $p < 0.05$); groups sharing the same letter are not significantly different. Boxes represent the median and interquartile range, with whiskers indicating the minimum and maximum values across the ten sample areas ($n = 10$).

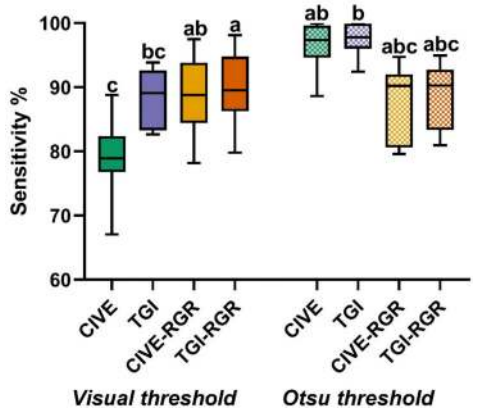


Fig. 7. Sensitivity (true positive rate, %) of the RGB index-based classification methods under visual and Otsu-based thresholding. Different letters above the boxes indicate statistically significant differences among groups (Dunn's test, $p < 0.05$); groups sharing the same letter are not significantly different. Boxes represent the median and interquartile range, with whiskers indicating the minimum and maximum values across the ten sample areas (n = 10).

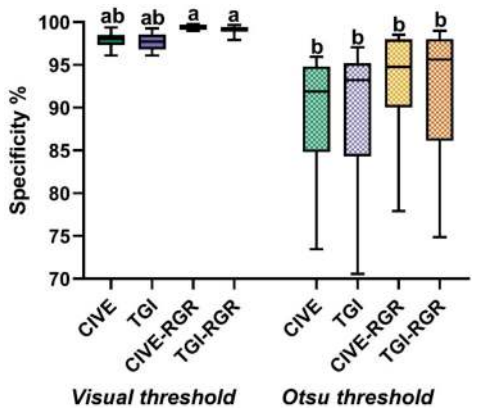


Fig. 8. Specificity (true negative rate, %) of the RGB index-based classification methods under visual and Otsu-based thresholding. Different letters above the boxes indicate statistically significant differences among groups (Dunn's test, $p < 0.05$); groups sharing the same letter are not significantly different. Boxes represent the median and interquartile range, with whiskers indicating the minimum and maximum values across the ten sample areas (n = 10).

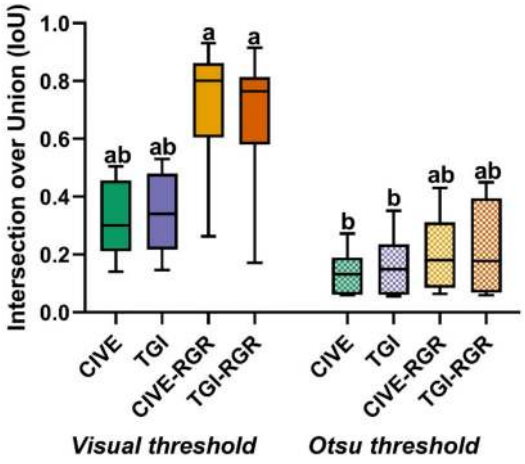


Fig. 9. Intersection over Union (IoU) values of the RGB index-based classification methods (CIVE, TGI, CIVE–RGR, and TGI–RGR) under visual and Otsu-based thresholding. Different letters above the boxes indicate statistically significant differences among groups (Dunn's test, $p < 0.05$); groups sharing the same letter are not significantly different. Boxes represent the median and interquartile range, with whiskers indicating the minimum and maximum values across the ten sample areas (n = 10).

exhibit strong spectral contrast during flowering. However; method selection should remain context-dependent and closely linked to species morphology; habitat structure; and monitoring objectives.The CIVE index; although originally developed under general conditions; performed reliably in the studied environment; indicating that strong floral contrast can compensate for the lack of local calibration. The consistent performance of all indices further supports the applicability of simple RGB-based metrics for detecting visually distinct flowering species. Previous work (Bakacsy et al., 2023) demonstrated that RGB indices such as TGI can be applied in a species-specific manner through threshold adjustment. In the present study; substantially higher accuracy (>99%; Tables 1 and 3) was achieved; likely due to the uniform yellow coloration and strong contrast of *Sedum* inflorescences compared to more heterogeneous species. Tabor (2022) applied UAV imagery combined with a random forest model using multiple indices and texture features; achieving high specificity (0.99) but lower sensitivity (0.77). In comparison; the present study achieved comparable performance using a simpler index-based approach; suggesting that complex models may not be necessary when target species exhibit strong spectral contrast. Similarly; de Sá et al. (2018) demonstrated the potential of UAV-based flower mapping; although their results were limited by species heterogeneity. In contrast; the compact structure and uniform coloration of *S. urvillei* subsp. *hillebrandtii* enabled more reliable detection using RGB indices. This is particularly relevant; as previous automated plant-counting approaches have typically relied on multispectral or hyperspectral sensors; which involve higher costs and more complex workflows (Jiménez López and Mulero-Pázmány, 2019; Reckling et al., 2021). This study contributes to the development of UAV-based monitoring methods for visually distinct flowering plant species, showing that simple, low-cost approaches can achieve comparable accuracy when the target species is spectrally distinct.

A key methodological insight of this study concerns the comparison between visually defined and automatically derived (Otsu-based) thresholds. While Otsu thresholding provides an objective and reproducible approach (Otsu, 1979); our results demonstrate that it does not necessarily lead to improved classification performance under all conditions. In particular; Otsu-based thresholding consistently increased

Table 3
Comparison of UAV-based plant monitoring studies using RGB or multispectral imagery for flowering plant detection and conservation monitoring.

Study	Target species	Sensor type	Methodological approach	Reported performance metric	Relative methodological complexity	Cost level
Present study	*Sedum urvillei* subsp. *hillebrandtii* (flowering patches)	RGB	RGB indices (CIVE, TGI) + negative masking (RGR); thresholding + GIS polygon operations	Overall accuracy up to 99.3%, specificity >99%; IoU (CIVE–RGR) 0.730 ± 0.198	Low	Low
Bakacsy et al. (2023)	*Asclepias syriaca*; *Gaillardia pulchella*	RGB	RGB vegetation indices (incl. TGI); species-specific thresholding; for *G. pulchella* inflorescences: shape-based index (IF)	Spatial overlap reported as ~60% (noted as lower than present study)	Moderate	Low
Bakó et al. (2024)	*Fritillaria meleagris* (flowering individuals)	RGB	Manual evaluation at very high spatial resolution	Detection accuracy 91–97%	High (labour-intensive)	Moderate
Gröschler and Oppelt (2022)	*Dactylorhiza majalis*	Multispectral	Vegetation index (MaVI) + random forest classification (incl. Feature-selection workflow as described in manuscript)	F1-score 0.99	High	High
Tabor (2022)	Floral cover (resource mapping for pollinators)	RGB (UAV imagery)	Random forest using 13 indices + texture features	Sensitivity 0.77, specificity 0.99	High	Moderate
de Sá et al. (2018)	*Acacia longifolia* (flowering)	RGB (UAV imagery)	Flower mapping from UAV imagery (workflow details not expanded in manuscript)	Weak correlation between field-observed and mapped flower counts	Moderate	Moderate
Reckling et al. (2021)	Rare plant monitoring (species not specified in manuscript text)	Not specified in manuscript	Species distribution model + AI-based object detection	Not specified in manuscript	High	High
Rominger and Meyer (2019)	Endangered plant census (species not specified in manuscript text)	Not specified in manuscript	UAV-based census methodology (details not expanded in manuscript)	Not specified in manuscript	Moderate	Moderate
Jiménez López and Mulero-Pázmány (2019)	Review (drones for conservation)	N/A	Review	N/A	Low	Low

Table 3. summarizes selected UAV-based plant monitoring studies cited in this manuscript, highlighting differences in target species, sensor type, analytical workflow, reported performance metrics, methodological complexity, and approximate cost requirements.

sensitivity; indicating a higher detection rate of true Sedum patches; but at the cost of reduced specificity; reflecting an increase in false positive detections. This trade-off can be explained by the characteristics of the vegetation index histograms. In the present study; the distributions were often unimodal or weakly bimodal due to the relatively small spatial extent of Sedum patches within the sample areas. Under such conditions; Otsu's method; which assumes separable class distributions; may fail to identify an optimal threshold and instead place it within overlapping value ranges (Xing et al., 2022; Mardanisamani and Eramian, 2022). This limitation of Otsu-based thresholding in unimodal histograms has been widely reported in remote sensing applications (Duarte et al., 2020; Rosin and Hervás, 2005), often resulting in increased misclassification and false positives. In contrast, visually defined thresholds were more conservative and better aligned with the biologically relevant spectral characteristics of the target species. This resulted in lower sensitivity but substantially higher specificity and overall classification reliability. This highlights that automated thresholding should be applied with caution in cases where class imbalance is pronounced.

Despite the high classification performance achieved under the tested conditions, several methodological limitations must be explicitly acknowledged. The survey was conducted on a single date during peak flowering under optimal illumination conditions. While this ensured strong chromatic contrast and image clarity, it limits the temporal robustness of the proposed thresholds. RGB-based vegetation indices are known to be sensitive to illumination angle, shadowing, and brightness variability (Hunt et al., 2011; Bendig et al., 2015; Zhou et al., 2008), and the absence of multi-date replication prevents evaluation of inter-annual or seasonal stability. The workflow was explicitly optimized for peak flowering. Consequently, only flowering individuals were detectable, whereas vegetative shoots were not captured by the RGB-based thresholds. The method therefore estimates flowering patch abundance rather than total population size. In years characterized by reduced or asynchronous flowering, detectability may decline substantially (Reckling et al., 2021). The temporal applicability of the approach is thus phenology-dependent and inherently narrow. The study also represents a single-species case within a relatively homogeneous open sandy grassland stand. The exceptionally high accuracy reflects the strong spectral distinctiveness of the uniformly yellow inflorescences. However; generalization to multispecies communities should be made cautiously. In habitats with simultaneous flowering taxa of similar chromatic properties; spectral overlap may increase the risk of misclassification (de Sá et al., 2018; Gröschler and Oppelt, 2022). Although RGR-based negative masking reduced false positives, it cannot fully eliminate confusion in spectrally complex communities. Environmental sensitivity further constrains transferability. Soil reflectance, heterogeneous background vegetation, mixed pixels, and cast shadows may alter index values, particularly for linear combinations such as CIVE and TGI (Caturegli et al., 2016; Bendig et al., 2015). Moreover, no radiometric calibration using reflectance panels was applied, and the workflow relied on relative digital numbers derived from the orthomosaic. While this enhances operational simplicity and cost-efficiency, it limits cross-site comparability and radiometric standardization. Taken together, the proposed method should be considered species-specific and context-dependent. Nevertheless, the conceptual framework – combining simple RGB indices with negative masking – may be transferable to other taxa characterized by compact growth form and strong chromatic contrast during flowering, provided that species-specific threshold validation is conducted.

In future research, this method could be combined with low-complexity but more advanced algorithms, such as object-based image analysis (OBIA), to enhance the integration of morphological filters (Blaschke et al., 2014). Subsequent investigations could encompass the adaptation of this technique to monitor invasive species (e.g.; for the purpose of early detection) or for the assessment of pollinator diversity and habitat conditions; as proposed by Tabor (2022). These results suggest that fully automated thresholding should be applied with

caution in ecological applications where class imbalance and spatial heterogeneity are pronounced.

5. Conclusion

S. urvillei subsp. *hillebrandtii* represents a characteristic species of well-preserved Pannonian sand steppe habitats. Because its populations are typically associated with structurally intact sandy grasslands, monitoring its spatial distribution can provide useful information on habitat quality and vegetation dynamics in these ecosystems. This study demonstrated that RGB-based UAV imagery combined with simple vegetation indices can reliably detect flowering individuals of *Sedum urvillei* subsp. *hillebrandtii* under favorable conditions. The application of RGR-based negative masking substantially improved classification performance, particularly by increasing specificity and reducing false positive detections. While automated Otsu thresholding increased sensitivity, it resulted in reduced classification stability compared to visually defined thresholds, highlighting a trade-off between detection rate and reliability. These findings indicate that expert-driven threshold selection may be more suitable in cases where the target species occupies a small proportion of the scene. The proposed workflow provides a cost-effective and operationally simple approach for conservation monitoring, particularly for species with strong spectral contrast during flowering. However, its applicability is limited by phenological constraints and environmental conditions, and therefore requires species-specific validation before broader application.

Supplementary data to this article can be found online at https://doi.org/10.1016/j.ecolind.2026.114888.

CRediT authorship contribution statement

László Bakacsy: Writing – review & editing, Writing – original draft, Visualization, Validation, Methodology, Investigation, Funding acquisition, Formal analysis, Data curation, Conceptualization. **Zalán Tobak:** Writing – review & editing, Validation, Funding acquisition, Formal analysis, Data curation. **László Mucsi:** Resources, Funding acquisition. **Boudewijn van Leeuwen:** Writing – review & editing, Supervision. **Csaba Biró:** Writing – review & editing, Conceptualization. **József Szatmári:** Writing – review & editing, Validation, Software, Resources, Methodology, Investigation, Funding acquisition, Formal analysis, Data curation, Conceptualization.

Declaration of competing interest

The authors declare that they have no known competing financial interests or personal relationships that could have appeared to influence the work reported in this paper.

Acknowledgments

The APC was funded by the University of Szeged Open Access Fund, grant number: 8332. This research was funded by the NKFIH-National Research and Innovation Office (NKFIH ADVANCED), grant number: 149686 and by grant TUDFO/47138-1/2019-ITM of the Ministry for Innovation and Technology, Hungary. The authors also thank the anonymous reviewers for their helpful critical comments and advice.

Data availability

The data supporting the findings of this study are available as supplementary material associated with this article.

References

Agisoft, LLC, 2020. Agisoft metashape user manual professional edition, version 1.5.4. Agisoft LLC, St. Petersburg, Russia.

Arok, M., Brkljač, B., Lugonja, P., Ivošević, B., Vukotić, M., Nikolić Lugonja, T., 2025. High resolution descriptors for UAV mapping in biodiversity conservation–A case study of sandy steppe habitat renewal. PLoS One 20, e0315399.

Bakacsy, L., Tobak, Z., Van Leeuwen, B., Szilassi, P., Biró, C., Szatmári, J., 2023. Drone-based identification and monitoring of two invasive alien plant species in open sand grasslands by six RGB vegetation indices. Drones 7, 207.

Bakó, G., 2013. Vegetációtérképezés Nagyfelbontású Valósszínes-és Multispektrális Légifelvételek Alapján. [Vegetation Mapping Based on High-Resolution True Colour and Multispectral Aerial Images]. Kitaibelia 18, 152–160 (in Hungarian with English abstract).

Bakó, G., Biró, É., Bódis, J., Búzás, E., 2024. A mocsári kockásliliom (*Fritillaria meleagris.* L.) levegőből történő tőszámlálásának feltételei. [Conditions for aerial counting of snake's head fritillary (*Fritillaria meleagris* L.) flowering individuals]. Bot. Közlem. 111, 269–275 (in Hungarian with English abstract).

Bates, T.H., Anderson, V.J., Johnson, R.L., Allphin, L., Rooks, D., Petersen, S.L., 2022. A. Practical assessment of using sUASs (drones) to detect and quantify wright fishhook cactus (*Sclerocactus wrightiae* LD Benson) populations in desert grazinglands. Land 11, 655.

Bendig, J., Yu, K., Aasen, H., Bolten, A., Bennertz, S., Broscheit, J., Gnyp, M.L., Bareth, G., 2015. Combining UAV-based plant height from crop surface models, visible, and near infrared vegetation indices for biomass monitoring in barley. Int. J. Appl. Earth Obs. Geoinf. 39, 79–87.

Biró, C., 2023. Personal communication. Kiskunsag National Park Directores, Liszt Ferenc utca 19, H-6000 Kecskemét, Hungary.

Blaschke, T., Hay, G.J., Kelly, M., Lang, S., Hofmann, P., Addink, E., Feitosa, Q.R., van der Meer, F., van der Werff, H., van Coillie, F., Tiede, D., 2014. Geographic object-based image analysis–towards a new paradigm. ISPRS J. Photogramm. Remote Sens. 87, 180–191.

Bölöni, J., Molnár, Z., Kun, A., 2011. Magyarország élőhelyei: vegetációtipusok leirása és határozója: ÁNÉR 2011. Hungary, MTA Ökológiai és Botanikai Kutatóintézete, Vácrátót, p. 439.

Borah, S., Anand, A., Sundaravadivel, P., Fletcher, R., Reddy, K., 2025. Unmanned Aerial Vehicle Solutions for Weed Detection in Precision Agriculture. IEEE Access.

Caturegli, L., Corniglia, M., Gaetani, M., Grossi, N., Magni, S., Migliazzi, M., Angelini, L., Mazzoncini, M., Silvestri, N., Fontanelli, M., Raffaelli, M., Peruzzi, A., Volterrani, M., 2016. Unmanned aerial vehicle to estimate nitrogen status of turfgrasses. PLoS One 11, e0158268.

Chaity, M.D., Eng, B., Irizarry, J., Saunders, G., Bhatta, R., Aardt, J.V., 2024. Evaluating the influence of imaging spectrometer system specifications on ecosystem spectral diversity assessment. In: AGU Fall Meeting Abstracts, 2024 (No. 32, pp. GC51CC-0032).

Cruzan, M.B., Weinstein, B.G., Grasty, M.R., Kohrn, B.F., Hendrickson, E.C., Arredondo, T.M., Thompson, P.G., 2016. Small unmanned aerial vehicles (micro-UAVs, drones) in plant ecology. App. Plant Sci. 4, 1600041.

De Sá, N.C., Castro, P., Carvalho, S., Marchante, E., López-Núñez, F.A., Marchante, H., 2018. Mapping the flowering of an invasive plant using unmanned aerial vehicles: is there potential for biocontrol monitoring? Front. Plant Sci. 9, 293.

Duarte, A., Acevedo-Muñoz, L., Gonçalves, C.I., Mota, L., Sarmento, A., Silva, M., Fabres, S., Borralho, N., Valente, C., 2020. Detection of longhorned borer attack and assessment in eucalyptus plantations using UAV imagery. Remote Sens. 12, 3153. https://doi.org/10.3390/rs12193153.

Gamon, J.A., Surfus, J.S., 1999. Assessing leaf pigment content and activity with a reflectometer. New Phytol. 143, 105–117.

Gröschler, K.C., Oppelt, N., 2022. Using drones to monitor broad-leaved orchids (*Dactylorhiza majalis*) in high-nature-value grassland. Drones 6, 174.

Hunt, E.R., Daughtry, C.S.T., Eitel, J.U.H., Long, D.S., 2011. Remote sensing leaf chlorophyll content using a visible band index. Agron. J. 103, 1090–1099.

International Crassulaceae Network (ICN). https://www.crassulaceae.ch/de/artikel?akID=182&aaID=2&aiID=U&aID=2626, 2025 (accessed 28 June 2025).

Jiménez López, J., Mulero-Pázmány, M., 2019. Drones for conservation in protected areas: Present and future. Drones 3, 10.

Kawashima, S., Nakatani, M., 1998. An algorithm for estimating chlorophyll content in leaves using a video camera. Ann. Bot. 81, 49–54.

Király, G., 2009. Új magyar füvészkönyv: Magyarország hajtásos növényei. In: [New Hungarian Herbal. The Vascular Plants of Hungary.]. Aggteleki Nemzeti Park Igazgatóság. Jósvafő, Hungary.

Liu, H.L., Lu, W.H., Chen, C., 2011. Research progress of grassland degraded succession and diagnosis. Acta Agrestia Sin. 19, 865.

Mardanisamani, S., Eramian, M., 2022. Segmentation of vegetation and microplots in aerial agriculture images: A survey. Plant Phenome J. 5, e20042. https://doi.org/10.1002/ppj2.20042.

Nowak, M.M., Dziób, K., Bogawski, P., 2018. Unmanned Aerial Vehicles (UAVs) in environmental biology: A review. Eur. J. Ecol. 4, 56–74.

Otsu, N., 1979. A threshold selection method from gray-level histograms. Automatica 11, 285–296. https://doi.org/10.1109/TSMC.1979.4310076.

QGIS Development Team, 2021. QGIS Geographic Information System. QGIS Association. https://www.qgis.org. (Accessed 17 June 2024).

Reckling, W., Mitasova, H., Wegmann, K., Kauffman, G., Reid, R., 2021. Efficient drone-based rare plant monitoring using a species distribution model and AI-based object detection. Drones 5, 110.

Rominger, K., Meyer, S.E., 2019. Application of UAV-based methodology for census of an endangered plant species in a fragile habitat. Remote Sens. 11, 719.

Rosin, P.L., Hervás, J., 2005. Remote sensing image thresholding methods for determining landslide activity. Int. J. Remote Sens. 26, 1075–1092. https://doi.org/10.1080/01431160512331330481.

Simon, T., 2000. A Magyarországi Edényes Flóra Határozója (Vascular Flora of Hungary) Nemzeti Tankönyvkiadó, Budapest, Hungary, p. 976.
Sipos, G., Tóth, O., Pécsi, E., Bíró, C., 2014. Bracketing the Age of freshwater carbonate formation by OSL dating near Lake Kolon, Hungary. J. Environ. Geogr. 7, 53–59. https://doi.org/10.2478/jengeo-2014-0012.
Sun, T., Xiao, L., Ata-Ul-Karim, S.T., Ma, Y., Zhang, W., 2025. Leveraging phenotyping and crop modeling in smart agriculture. Front. Plant Sci. 16, 1626622.
Tabor, J.A., 2022. Quantifying Floral Resource Availability Using Unmanned Aerial Systems and Machine Learning Classifications to Predict Bee Community Structure (Master's thesis, Utah State University).
Tóth, K., 1996. 20 éves a Kiskunsági Nemzeti Park 1975–1995. Kiskunság Nemzeti Park Igazgatósága, Kecskemét, Hungary, p. 234.
Wang, Z., Jiang, L., Wang, S., Wang, Y., Zhou, H., 2022. Assessment methods for grassland restoration. Acta Ecol. Sin. 42, 6464–6473.
Wang, Y., Wan, H., Hu, Z., Gao, J., Sun, C., Yang, B., 2024. *Artemisia frigida* distribution mapping in grassland with unmanned aerial vehicle imagery and deep learning. Drones 8, 151.
Xing, H., Zhu, L., Chen, B., Liu, C., Niu, J., Li, X., Feng, Y., Fang, W., 2022. A comparative study of threshold selection methods for change detection from very high-resolution remote sensing images. Earth Sci. Inf. 15, 369–381. https://doi.org/10.1007/s12145-021-00734-y.
Zhang, Y.J., Zhu, J.T., Shen, R.N., Wang, L., 2020. Research progress on the effects of grazing on grassland ecosystem. Chin. J. Plant Ecol. 44, 553.
Zhou, W., Troy, A., Grove, M., 2008. Object-based land cover classification and change analysis in the Baltimore metropolitan area using multitemporal high resolution remote sensing data. Sensors 8, 1613–1636.